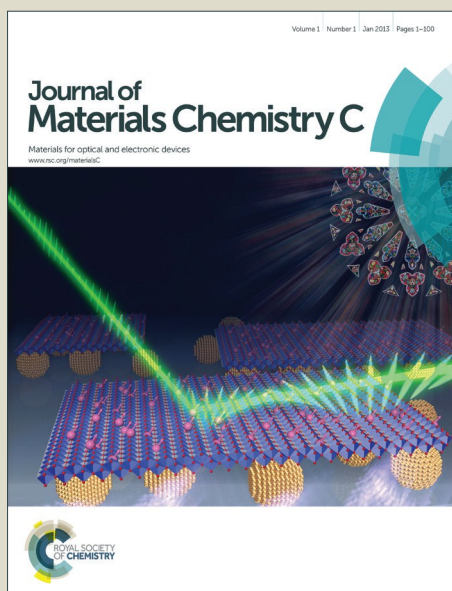


# Journal of Materials Chemistry C

Accepted Manuscript



This is an *Accepted Manuscript*, which has been through the Royal Society of Chemistry peer review process and has been accepted for publication.

*Accepted Manuscripts* are published online shortly after acceptance, before technical editing, formatting and proof reading. Using this free service, authors can make their results available to the community, in citable form, before we publish the edited article. We will replace this *Accepted Manuscript* with the edited and formatted *Advance Article* as soon as it is available.

You can find more information about *Accepted Manuscripts* in the [Information for Authors](#).

Please note that technical editing may introduce minor changes to the text and/or graphics, which may alter content. The journal's standard [Terms & Conditions](#) and the [Ethical guidelines](#) still apply. In no event shall the Royal Society of Chemistry be held responsible for any errors or omissions in this *Accepted Manuscript* or any consequences arising from the use of any information it contains.

# Observation of a nanoscale phase separation in blue-emitting Ce-doped SiO<sub>1.5</sub> thin films

*J. Weimmerskirch-Aubatin<sup>a</sup>, M. Stoffel<sup>a,\*</sup>, X. Devaux<sup>a</sup>, A. Bouché<sup>a</sup>, G. Beainy<sup>b</sup>, E. Talbot<sup>b</sup>,*

*P. Pareige<sup>b</sup>, Y. Fagot-Révurat<sup>a</sup>, M. Vergnat<sup>a</sup>, H. Rinnert<sup>a</sup>*

*<sup>a</sup> Université de Lorraine, UMR CNRS 7198, Institut Jean Lamour, BP 70239,*

*54506 Vandœuvre-lès-Nancy, France*

*<sup>b</sup> Groupe de Physique des Matériaux, UMR CNRS 6634, Université et INSA de Rouen,*

*BP 12, Avenue de l'Université,*

*76801 Saint Etienne de Rouvray, France*

\*Corresponding author: Mathieu Stoffel, e-mail : [mathieu.stoffel@univ-lorraine.fr](mailto:mathieu.stoffel@univ-lorraine.fr)

## Abstract

Both the optical and structural properties of Ce-doped SiO<sub>1.5</sub> thin films were investigated. The Ce-related blue luminescence, which can be even seen at room temperature for as-grown films, exhibits a rather complex evolution with the annealing temperature. In particular, a strong decrease is observed when the films are annealed at 900°C. Structural characterizations combining scanning transmission electron microscopy and atom probe tomography reveal the formation of Si- and Ce-rich clusters at this temperature thus demonstrating that the decreasing Ce-related luminescence is due to concentration induced quenching. For annealing temperatures larger than 900°C, the Ce-related luminescence increases. The different structural characterizations provide clear experimental evidence of a phase separation occurring at the nanoscale between pure Si nanocrystals and Ce-rich clusters having a

stoichiometry close to the cerium silicates  $\text{Ce}_2\text{Si}_2\text{O}_7$  or  $\text{Ce}_{4.667}(\text{SiO}_4)_3\text{O}$ . The latter compounds are optically active thereby explaining the increased Ce-related luminescence observed at the highest annealing temperature.

## Introduction

Since bulk Si is an indirect bandgap semiconductor, getting light out of Si-based materials is a challenging issue, not only in the infrared for telecommunications applications but also in the visible range for displays and white light electroluminescent diodes. At the nanometer scale, the charge carriers are confined in three dimensions, and pure Si nanocrystals embedded in either a  $\text{SiO}_2$ <sup>1</sup> or a  $\text{Si}_3\text{N}_4$ <sup>2</sup> matrix are shown to emit light in the visible-near infrared even at room temperature. Moreover, it was shown that a good control of the Si nanocrystal size can be achieved in  $\text{SiO}/\text{SiO}_2$  multilayers allowing thus to tune their emission wavelength in the red-near infrared range.<sup>3,4</sup> The optical properties of Si-based materials containing Si nanocrystals can be further adjusted by doping the  $\text{SiO}_x$  ( $0 < x < 2$ ) matrix with optically active lanthanide ions. The first studies have concerned the  $\text{Er}^{3+}$  doping of  $\text{SiO}_x$  thin films, which is of potential interest for telecommunications.<sup>5</sup> More recently, other authors have also studied the doping of  $\text{SiO}_x$  thin films with  $\text{Nd}^{3+}$  ions for photovoltaic applications.<sup>6,7</sup> In both cases, an efficient energy transfer was found to occur between Si nanocrystals and  $\text{Er}^{3+}$  or  $\text{Nd}^{3+}$  ions thereby enhancing the rare earth based luminescence. If many results were reported for light emission in red and infrared, few results were published for a blue emission in Si-based materials. Among all rare earth elements, Ce is of particular interest since it is characterized by an allowed electric dipolar  $5d-4f$  transition giving rise to emission in the violet-blue range. This property may be of interest for the development of blue light emitting diodes fully compatible with the Si technology. Morshed et al.<sup>8</sup> obtained violet-blue luminescence in  $\text{CeO}_2$  films epitaxially grown on Si(111) substrates by pulsed laser deposition and subsequently

annealed at 1000°C in Ar ambient. The luminescence was tentatively attributed to the formation of a  $\text{Ce}_6\text{O}_{11}$  compound. Later, Choi et al.<sup>9</sup> reported violet/blue luminescence in cerium oxide films grown by radio-frequency sputtering directly on Si(001) substrates. The luminescence was attributed to the formation of cerium silicates. Similar observations were made by Kepinski et al.<sup>10</sup> in  $\text{CeO}_2$ - $\text{SiO}_2$  films prepared by the sol-gel method and by Li et al.<sup>11</sup> in Ce-doped silicon oxide thin films grown by electron cyclotron resonance plasma enhanced chemical vapor deposition. By investigating Ce-doped  $\text{SiO}_{1.5}$  films prepared by evaporation, we found that  $\text{Ce}^{3+}$  ions are mainly directly excited with only a negligible influence of Si nanocrystals.<sup>12</sup> Finally, strong blue luminescence was also reported recently in Ce-doped  $\text{SiO}_2$  thin films prepared by evaporation.<sup>13</sup>

While extensive work has been already performed particularly regarding the optical properties of rare earth doped  $\text{SiO}_x$  thin films, several critical issues remain still unsolved. In particular, the spatial localization of the rare earth ions with respect to the Si nanocrystals has not yet been addressed. For example, it is not yet clear whether the rare earth ions are located in or at the surface/periphery of the nanocrystals. Moreover, the influence of the rare earth ions on the Si nanocrystal formation has not yet been studied.

In this paper, we investigate the optical and structural properties of Ce-doped  $\text{SiO}_{1.5}$  thin films. For all the Ce contents investigated, the Ce-related luminescence follows a similar evolution as a function of the annealing temperature. At 900°C, a strong decrease of the PL intensity is observed. Structural characterization tools show that both Ce and Si form clusters located at the same position thus explaining the decreasing luminescence by concentration induced quenching. For annealing temperatures beyond 980°C, we observe at some locations the beginning of a separation between Ce-rich clusters and Si nanocrystals. At 1100°C, we report the first observation of a phase separation occurring at the nanoscale between pure Si nanocrystals and Ce-rich clusters having a stoichiometry close to the cerium silicates

$\text{Ce}_2\text{Si}_2\text{O}_7$  or  $\text{Ce}_{4.667}(\text{SiO}_4)_3\text{O}$ . These compounds are known to be luminescent thereby explaining the reappearance of the Ce-related luminescence at this temperature.

## Experimental

The  $\text{SiO}_{1.5}$  films were obtained by co-evaporation on Si(001) or fused silica substrates held at room temperature of SiO powder from a thermal cell and  $\text{SiO}_2$  from an e-beam gun in an ultra-high vacuum chamber. The Ce doping was performed by a Knudsen cell heated at  $\sim 1400^\circ\text{C}$ . The Ce flux was monitored by a quartz microbalance and the Ce content defined by  $[\text{Ce}]/([\text{Si}]+[\text{O}]+[\text{Ce}])$  was varied between 0.3 % and 4 %. The film thickness was 20 nm for the samples investigated by transmission electron microscopy and 200 nm for all other samples considered in this study. The samples were post-grown annealed in either a tubular oven for temperatures between  $500^\circ\text{C}$  and  $900^\circ\text{C}$  or in a rapid thermal annealing furnace in  $\text{N}_2$  atmosphere at  $1100$ - $1200^\circ\text{C}$ . In the case of the tubular oven, the temperature was ramped up with a rate of  $10^\circ\text{C}/\text{min}$  up to the desired temperature prior to cooling down while for the rapid thermal annealing furnace all samples were kept at  $1100^\circ\text{C}$ - $1200^\circ\text{C}$  during 5 min. The steady state photoluminescence (PL) was excited with a 325 nm He-Cd laser and subsequently analyzed by a monochromator equipped with a 600 grooves/mm grating and measured by a photomultiplier tube operating in the UV-visible range. A Xe lamp (maximum power 300 W) was used as excitation source for the photoluminescence excitation (PLE) measurements. The response of the detection system was precisely calibrated by a tungsten wire calibration source. The Raman spectra were collected in backscattering geometry using a 532 nm laser diode as excitation source. The scattered light was dispersed by a grating with 1800 grooves/mm and detected by a multichannel charge coupled device (CCD) camera cooled at 200 K. All Raman measurements were performed on samples deposited on fused silica substrates in order to get rid of the contribution of the transverse optical phonon line of

the Si substrate. The X-ray photoelectron spectra were measured using the non-monochromatized  $\text{AlK}_{\alpha}$  radiation at 1486.6 eV. Prior to the measurements, the samples were subjected to a 45 min  $\text{Ar}^{+}$  ion bombardment in order to remove potential impurities/contaminants from the surface. The photoelectrons were collected by a Scienta SES 200 hemispherical analyzer. The overall resolution of the setup was about 0.8 eV. The structural properties of the samples were studied by high-resolution transmission electron microscopy (HRTEM) and scanning transmission electron microscopy (STEM) with a JEOL ARM200F. STEM images were simultaneously recorded using high angle annular dark field (HAADF) and bright field (BF) detectors and completed with local energy-dispersive X-ray spectroscopy (EDS). To avoid any phase precipitation due to ion or electron beam damages, the samples were mechanically thinned up to the electron transparency by the tripod method. Both TEM and STEM investigations were performed at 80 kV. The 3D mapping of the distribution of atoms in the sample was obtained by laser-assisted atom probe tomography (APT) analyses. The tips required for the APT analysis were prepared according to a process used on similar materials as reported elsewhere.<sup>14,15</sup> The analyses were carried out at 80 K using a CAMECA LAWATAP instrument with an amplified Ytterbium doped laser emitting at a wavelength of 343 nm providing a 350 fs pulse duration and a 100 KHz repetition rate with an energy per pulse around 50 nJ. The infrared absorption spectra are obtained using a Fourier transform infrared absorption spectrometer (FTIR). The films are analyzed at normal incidence by direct transmission. The acquisition of the spectra is performed in absorbance mode. The spectra of the thin films are obtained after subtraction of the reference spectrum measured on a Si substrate. In order to compare the obtained results, a baseline is subtracted from each spectrum to eliminate the interference fringes caused by multiple reflections in the substrate.

## Results and discussion

Figure 1(a) displays a typical room temperature (RT) steady state PL spectrum of an as-deposited  $\text{SiO}_{1.5}$  thin film doped with 3% Ce (red solid line). We observe strong blue luminescence, which can be even seen with the naked eye (see inset of Fig. 1(a)).

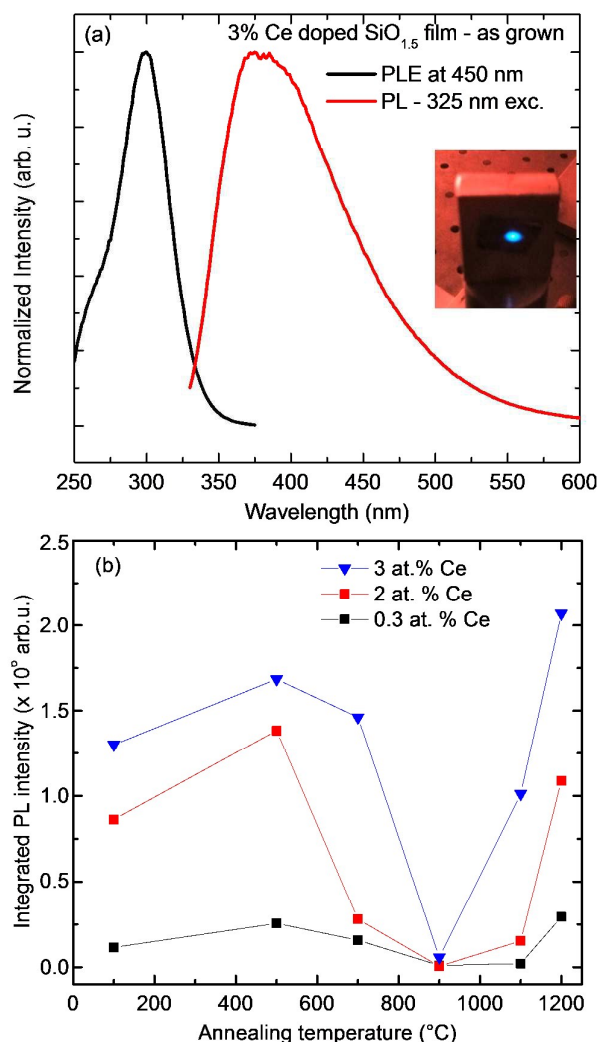


**Fig.1** Steady state PL spectrum of a 3% Ce-doped  $\text{SiO}_{1.5}$  thin film measured at room temperature (red solid line). The corresponding PLE spectrum is shown as a black solid line. The inset shows a photograph of the sample showing the blue luminescence visible with the

naked eyes. (b) Integrated Ce-related PL intensity as a function of annealing temperature for three different Ce contents.

The PL band is rather broad and extends from 330 nm to 530 nm with a maximum centered at  $\sim 380$  nm. The luminescence may be due either to defects of the  $\text{SiO}_{1.5}$  matrix or to the allowed electric dipolar  $5d-4f$  transition of isolated  $\text{Ce}^{3+}$  ions. The former hypothesis can, however, be ruled out since an as-grown and undoped  $\text{SiO}_{1.5}$  film does not show any luminescence near 400 nm. Moreover, the PL intensity increases with the Ce content in the films (see also Fig. 1(b)). We can therefore unambiguously attribute the observed luminescence to the allowed electric dipolar  $5d-4f$  transition of  $\text{Ce}^{3+}$  ions. In order to determine the excitation mechanism of  $\text{Ce}^{3+}$  ions, we further perform PLE measurements. In this case, the detection wavelength is fixed at 450 nm (this wavelength has been chosen since detection is possible for both as-grown and annealed samples for which the PL signal shifts to higher wavelengths, see also Supporting Information) and the excitation wavelength is varied between 250 nm and 370 nm. The PLE spectrum, which is shown in Fig. 1(a) as a black solid line, is characterized by a single peak centered at  $\sim 300$  nm. This peak is typical for the excitation of the  $5d$  levels of  $\text{Ce}^{3+}$  ions starting from the fundamental  $^2F_{5/2}$  level thus showing that  $\text{Ce}^{3+}$  ions are mainly directly excited. In the following, we will concentrate our attention to the Ce-related luminescence and its evolution with the annealing temperature. Figure 1(b) displays the evolution of the integrated Ce-related luminescence as a function of the annealing temperature. It is noteworthy that the evolution follows the same trend independently of the Ce concentration in the films. One can easily distinguish three different regimes. Firstly, from RT up to  $500^\circ\text{C}$ , the integrated luminescence increases. Secondly, from  $500^\circ\text{C}$  up to  $900^\circ\text{C}$ , the integrated luminescence decreases and eventually reaches a minimum at  $900^\circ\text{C}$ . Thirdly, at higher annealing temperatures up to  $1200^\circ\text{C}$ , the integrated Ce-related luminescence increases. It is important to note that the reappearance of the PL and the existence of a

minimum of PL intensity are not due to the annealing treatment method. Indeed, we carefully checked that a similar qualitative evolution is obtained when the samples are annealed using only the RTA furnace with a minimum of PL intensity occurring at a higher annealing temperature, i.e. 1100°C. A similar qualitative evolution has been already reported by Li et al.<sup>11</sup> in Ce-doped silicon oxide films but the evolution has not been investigated in details. Interestingly, as the annealing temperature increases, the Ce-related luminescence band shifts to higher wavelength (see Supporting Information). Let us consider the first regime, i.e. from RT up to 500°C. It is well known that annealing heals out point defects thus leading to a decreased density of non-radiative recombination centers. Consequently, the luminescence increases as observed in Fig. 1(b). We will now consider the second regime corresponding to annealing temperatures between 500°C and 900°C. Li et al.<sup>11</sup> have interpreted the observed decrease by precipitation of Ce<sup>3+</sup> ions but the existence of Ce rich clusters is unclear and the chemical composition of the clusters remains unknown. Different hypotheses can be put forward to explain the decreased PL intensity. The first one is a modification of the valence of Ce ions evolving from Ce<sup>3+</sup> ions to Ce<sup>4+</sup> ions. The latter are known not to be optically active which could possibly result in a quenching of the luminescence. The second one is that Ce ions diffuse and form clusters leading to a concentration induced quenching of the luminescence. In order to test the possibility of valence changes, X-ray photoelectron spectroscopy (XPS) measurements of the Ce 3*d* core level were carried out. The different valence states are characterized by well-defined peaks appearing at different binding energies thus allowing discriminating between Ce<sup>3+</sup> and Ce<sup>4+</sup>.<sup>16, 17</sup>

Figure 2 shows the Ce 3*d* core levels measured on a 3% Ce-doped SiO<sub>1.5</sub> thin film annealed at 500°C (Fig. 2(a)) and at 900°C (Fig. 2(b)). The obtained spectra look qualitatively similar to those previously measured on thin CeO<sub>2</sub> films deposited on either Si(111) substrates<sup>17</sup> or thin Pt foils.<sup>16</sup> After subtraction of a Shirley background,<sup>18, 19</sup> both spectra were fitted

with Gaussian-Lorentzian functions to de-convolve multiple peaks that are closely spaced in binding energy. The spin-orbit splitting between the Ce  $3d_{3/2}$  and the Ce  $3d_{5/2}$  peaks was fixed at 18.3 eV as in previous works.<sup>16, 17</sup> The fitting was performed by using the chemical shifts from the literature<sup>16, 17</sup> and by varying only the height and full width at half maximum (FWHM) of the peaks. The ratio between the Ce<sup>3+</sup> and Ce<sup>4+</sup> related peak intensities was then used to determine the amount of Ce ions in the (III)/(IV) oxidation state. In both cases, the contribution of Ce<sup>3+</sup> ions is dominant and only a moderate increase of the Ce<sup>4+</sup> content is observed when the annealing temperature increases from 500°C to 900°C. We can thus rule out a valence state change as the main origin of the decreased PL intensity observed at 900°C. To test whether Ce clusters may form, STEM measurements were performed.

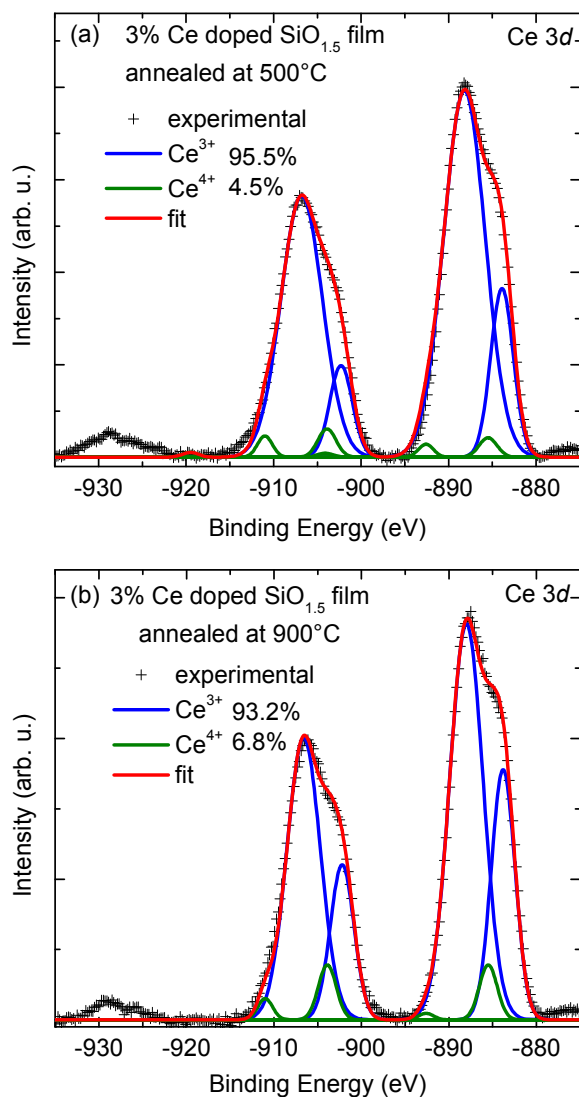


**Fig.2** X-ray photoelectron spectra of the Ce 3d core level measured on a 3 % Ce-doped SiO<sub>1.5</sub> thin film after annealing at 500°C (a) and 900°C (b). The result of the fit (solid lines) is superimposed on the experimental data (crosses).

Figure 3 (a) shows a HAADF image of a 3% Ce-doped SiO<sub>1.5</sub> thin film annealed at 900°C and the corresponding bright field image is shown Figure 3(b). One can clearly identify a high density of clusters which exhibit a high contrast (bright on HAADF and dark on BF). This observation suggests that they are composed of a heavy element which in our case is Ce. Spatially resolved EDS investigations (Figure 3(c) and 3(d)) show that the clusters

contain Ce while the surrounding matrix is Ce-free. Moreover, the analysis of the HRSTEM images shows that these clusters are amorphous. The demonstration of the formation of Ce-rich clusters allows us to conclude that the decreased PL intensity observed at 900°C is the result of concentration induced quenching. If we assume that all Ce ions are randomly distributed in the as-grown films, the observation of Ce clusters in the 900°C annealed sample indicates that a significant Ce diffusion must have taken place during annealing. We cannot exclude that other atomic species of lower mass like Si may also diffuse during high temperature annealing. In order to test the possibility of Si diffusion, we have performed atom probe tomography on the 3% Ce-doped  $\text{SiO}_{1.5}$  thin film annealed at 900°C.

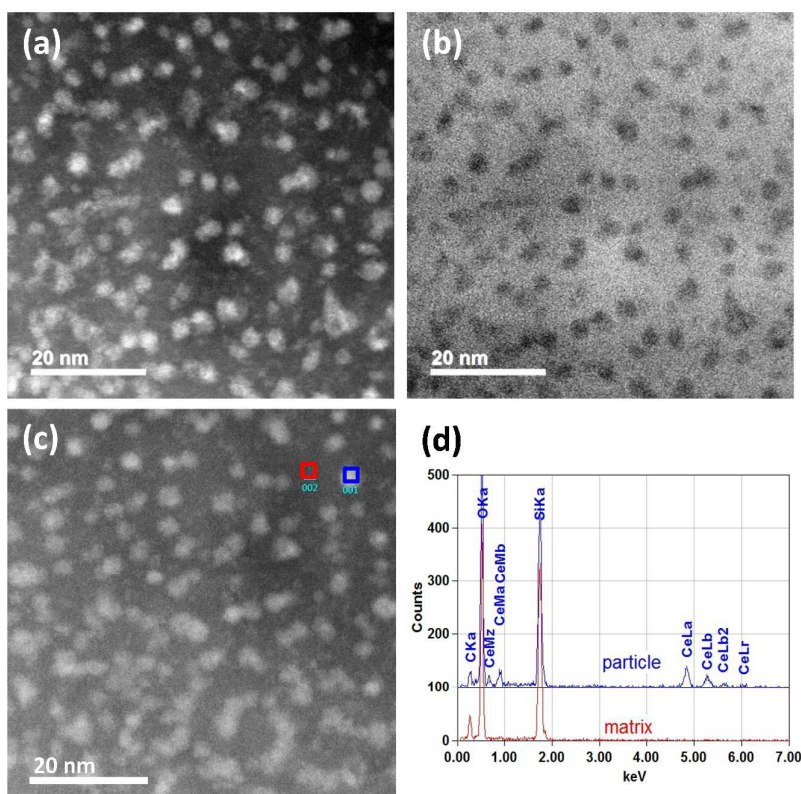


**Fig.3** HAADF image of a 3% Ce-doped  $\text{SiO}_{1.5}$  thin film annealed at 900°C showing the presence of Ce-rich clusters (a) and corresponding bright field image (b). HAADF image (c) showing the areas (red square for the matrix and blue square for a particle) used for the EDS analysis (d)

Figure 4(a) shows a typical slice view ( $48.8 \times 48.8 \times 5 \text{ nm}^3$ ) taken from the 3D reconstructed volume representing Si atoms for the sample annealed at  $900^\circ\text{C}$ . Oxygen atoms are not represented for clarity reasons. The cartography clearly reveals an inhomogeneous Si distribution with the presence of Si-rich clusters. In contrast, the as-grown sample exhibits a rather uniform Si distribution (not shown here). The presence of Si-rich clusters in the sample annealed at  $900^\circ\text{C}$  thus indicates that the demixtion of the  $\text{SiO}_{1.5}$  film has already started. The Si atoms in excess -by comparison with  $\text{SiO}_2$ - will diffuse and eventually agglomerate to form the observed clusters as known for undoped  $\text{SiO}_x$  films.<sup>20, 4</sup> Figure 4(b) shows the Ce atoms in the same slice view ( $48.8 \times 48.8 \times 5 \text{ nm}^3$ ). The cartography gives evidence of the presence of Ce-rich clusters thus confirming the previous STEM observations. Interestingly, showing both Si- and Ce-related maps (Fig. 4(c)), we found that Ce-rich and Si-rich clusters are located on the same position. Thus, it seems that Ce atoms do not prevent the demixtion of the  $\text{SiO}_{1.5}$  film but instead leads to the formation of Si-clusters containing Ce. Although we have not investigated in detail the diffusion mechanism of both Si and Ce atoms, we can nevertheless suggest that both atomic species will probably migrate to the pores/vacancies contained in the amorphous  $\text{SiO}_{1.5}$  thin films. At the present stage of our investigation, it is not yet clear whether the Si-rich clusters are crystallized or not. To answer this question, Raman measurements have been carried out.

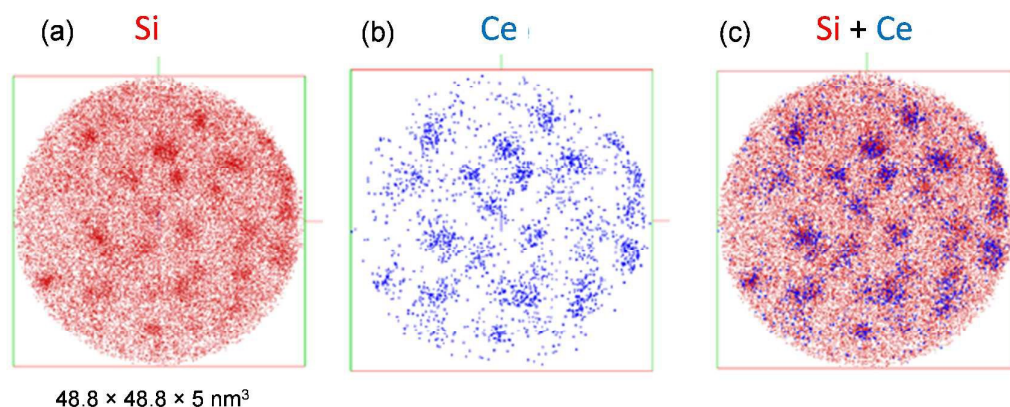


**Fig.4** Atom probe tomography analysis of the 3% Ce-doped  $\text{SiO}_{1.5}$  thin film annealed at  $900^\circ\text{C}$ . (a) Plane view of a 5 nm thick slice taken from the reconstructed volume. The Si atoms are shown as red dots, providing evidence of the presence of Si-rich clusters, (b) Analogous plane view showing Ce atoms as blue dots, evidencing the presence of Ce-rich clusters, (c) Superposition of the maps shown in (a) and (b) demonstrating that both Si and Ce-rich clusters have the same locations. All the views have the size  $48.8 \times 48.8 \times 5 \text{ nm}^3$ .

Figure 5 displays the Raman spectra of a 3% Ce-doped  $\text{SiO}_{1.5}$  film measured for different annealing temperatures ranging from  $900^\circ\text{C}$  to  $1150^\circ\text{C}$ . When the film is annealed at  $900^\circ\text{C}$ , the Raman spectrum looks very similar to that of a fused silica substrate indicating that the crystallization of the Si atoms in excess has not yet started. Indeed the Raman response of amorphous silicon is characterized by a broad and weak peak located at around  $480 \text{ cm}^{-1}$ . The absence of Raman signature of the film is interpreted by the presence of silicon in its amorphous state. In contrast, as the film is annealed at  $1025^\circ\text{C}$ , a small peak emerges at  $\sim 520 \text{ cm}^{-1}$ , i.e. very close to the position of the transverse optical phonon in bulk crystalline Si ( $520.5 \text{ cm}^{-1}$ ). We thus conclude that pure Si nanocrystals start to form at temperatures higher than  $980^\circ\text{C}$ . A similar evolution is observed for a 0.7 % Ce-doped  $\text{SiO}_{1.5}$  film (not shown here). Moreover, the intensity of the peak observed at  $520 \text{ cm}^{-1}$  increases as the annealing temperature increases (see inset of Fig. 5) thus suggesting the formation of a larger number of pure Si nanocrystals. This result is quite surprising since we have shown in Fig. 4 (c) that Ce

ions have the same locations than Si atoms. One could thus expect the formation of a Ce-Si-O compound rather than the formation of pure Si nanocrystals. To understand further the evolution of the system, in particular the distribution of the Ce ions in the sample annealed at 980°C, atom probe tomography experiments were further performed on the 3% Ce-doped  $\text{SiO}_{1.5}$  thin film annealed at 980°C.

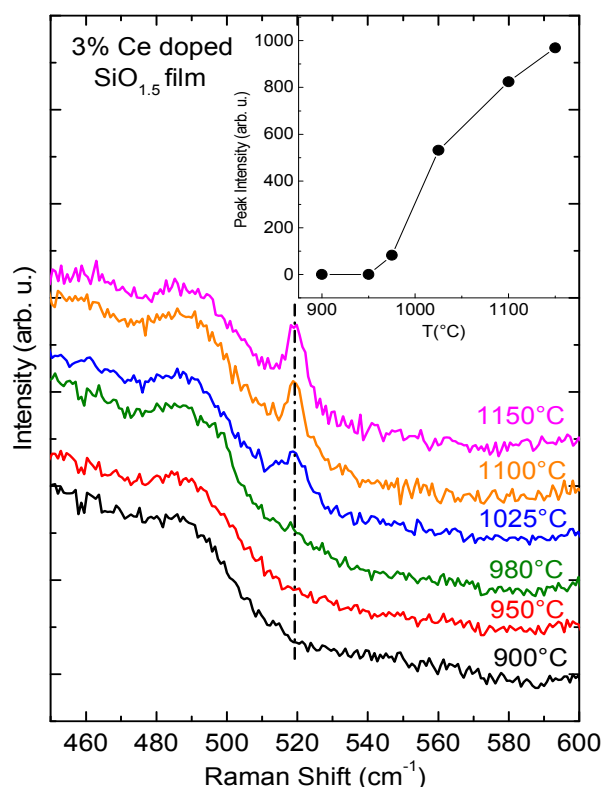


**Fig.5** Raman spectra measured on a 3% Ce-doped  $\text{SiO}_{1.5}$  thin film after annealing at various temperatures between 900°C and 1150°C. All spectra are vertically offset for clarity. The vertical dashed–dotted line indicates the position of the crystalline Si-TO peak at 520  $\text{cm}^{-1}$ . The inset shows the evolution of the integrated Raman peak intensity at 520  $\text{cm}^{-1}$  as a function of annealing temperature.

Figure 6(a) shows a typical slice view ( $33 \times 33 \times 5 \text{ nm}^3$ ) taken from the reconstructed volume representing Si atoms. Similarly to the sample annealed at 900°C, the distribution of

Si atoms is still inhomogeneous. The same is valid for Ce ions (Fig. 6(b)) as observed previously (Fig. 4(b)). If one shows both Si and Ce-related atomic maps (Fig. 6(c)), we can recognize that, at some locations, the Ce-rich regions start to be separated from the Si nanocrystals as shown by the dashed circles in Fig. 6(c). It would be now interesting to understand how the system evolves at even higher annealing temperatures, for instance at 1100°C where the Ce-related luminescence is found to increase (Fig. 1(b)). We thus perform a similar analysis on the 3% Ce-doped  $\text{SiO}_{1.5}$  thin film annealed at 1100°C.

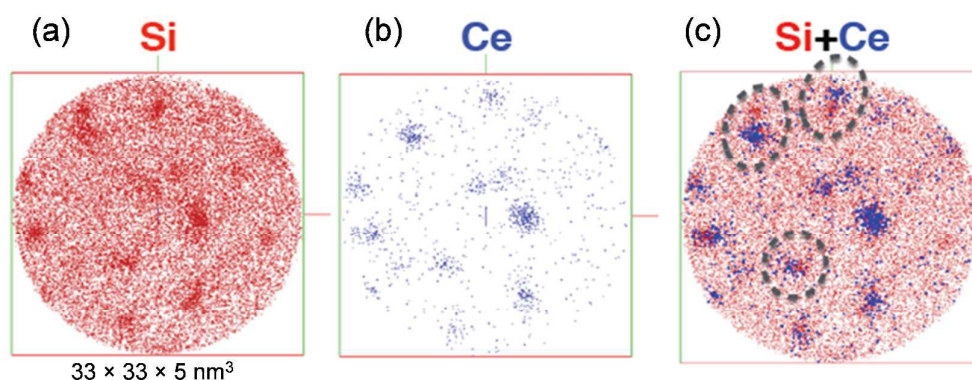


**Fig.6** Atom probe tomography analysis of the 3% Ce-doped  $\text{SiO}_{1.5}$  thin film annealed at 980°C. (a) Plane view of a 5 nm thick slice taken from the reconstructed volume. The Si atoms are shown as red dots, providing evidence of the presence of Si-rich clusters, (b) Analogous plane view showing Ce atoms as blue dots, evidencing the presence of Ce-rich clusters, (c) Superposition of the maps shown in (a) and (b) demonstrating that both Si and Ce-rich clusters do not longer have the same locations (also indicated by dashed circles). All the views have the size  $33 \times 33 \times 5 \text{ nm}^3$ .

Figure 7(a) shows a typical slice view ( $30 \times 30 \times 5 \text{ nm}^3$ ) taken from the reconstructed volume and representing both Si atoms (red dots) and Ce atoms (blue dots). While at 980°C we observe the beginning of a separation between pure Si nanocrystals and Ce-rich clusters, at 1100°C, the phase separation seems now to be almost complete. Indeed, the center of mass of the Si nanocrystals does not longer coincide with the center of mass of the Ce-rich clusters.

This is the first experimental evidence of a phase separation occurring at a length scale below 10 nm in rare earth doped silicon oxide thin films. We then further used atom probe tomography to get a better insight in the composition of the Ce-rich clusters. The compositional analysis reveals that these clusters are indeed composed of Ce but also of Si and O with relative amounts 16.3%, 18.2 % and 65.5 %, respectively. The composition of these clusters appears to be compatible with the formation of cerium silicates of stoichiometry  $\text{Ce}_2\text{Si}_2\text{O}_7$  and  $\text{Ce}_{4.667}(\text{SiO}_4)_3\text{O}$ . The latter compounds are known to be luminescent in the violet/blue range.<sup>9,11</sup> This eventually explains the reappearance of the Ce-related luminescence for samples annealed at 1100°C (third regime in Fig. 1(b)). Finally, in order to further strengthen our observations, we investigate the structural properties of the 3% Ce-doped  $\text{SiO}_{1.5}$  film annealed at 1100°C by transmission electron microscopy (TEM). Figure 7(b) shows a high resolution TEM image providing evidence of a phase separation between a pure Si nanocrystal (circled in red) and a Ce-rich cluster located in its vicinity (circled in blue). The latter is not sufficiently well-oriented to clearly evidence crystal planes on the micrograph. Nevertheless both STEM HAADF and STEM BF have shown that the Ce-rich clusters are crystalline. However, the main grains appear twinned or polycrystalline, this makes a structural determination difficult starting from HRSTEM micrographs. For the few monocrystalline grains that were observed, the coexistence of both crystalline  $\text{Ce}_{4.667}(\text{SiO}_4)_3\text{O}$  and  $\text{Ce}_2\text{Si}_2\text{O}_7$  compounds cannot be excluded in agreement with the Ce-Si-O phase diagram.

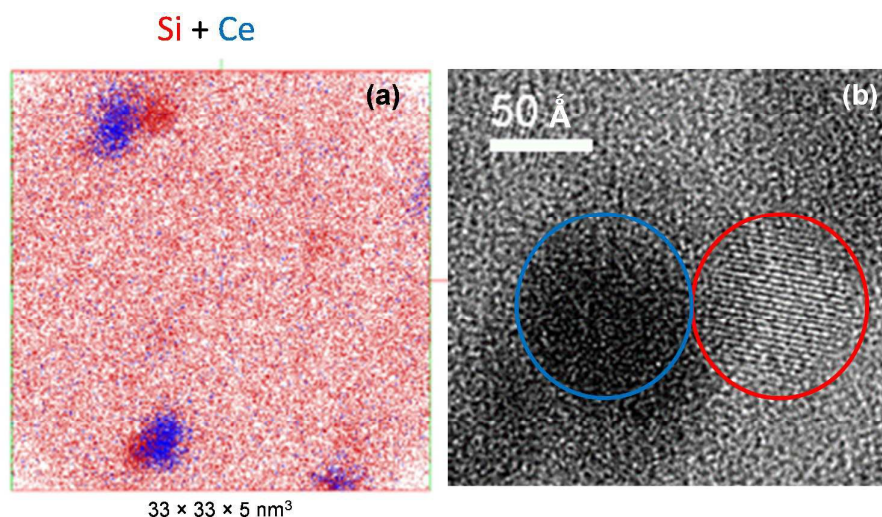


**Fig.7** Atom probe tomography analysis of the 3% Ce-doped  $\text{SiO}_{1.5}$  thin film annealed at  $1100^\circ\text{C}$ . (a) Plane view ( $30 \times 30 \times 5 \text{ nm}^3$ ) of a 5 nm thick slice taken from the reconstructed volume showing both Si atoms (red dots) and Ce atoms (blue dots). The phase separation between pure Si nanocrystals and Ce-rich clusters is evident. (b) High resolution cross sectional TEM image showing the presence of a pure Si nanocrystal (circled in red) in the immediate vicinity of a Ce-rich cluster (circled in blue).

To further confirm the formation of a cerium silicate, we investigate the Ce-doped  $\text{SiO}_{1.5}$  film annealed at  $1200^\circ\text{C}$  by FTIR spectroscopy. Figure 8 displays the FTIR spectra of Ce-doped  $\text{SiO}_{1.5}$  films annealed at  $1200^\circ\text{C}$  for different Ce concentrations ranging from 0.3 % to 4 %. All spectra are dominated by well-defined lines at  $800 \text{ cm}^{-1}$  corresponding to the symmetric stretching mode of the Si-O-Si bond and at  $1080 \text{ cm}^{-1}$  corresponding to the asymmetric stretching mode of the Si-O-Si bond in  $\text{SiO}_2$ .<sup>22,23</sup> Apart from these lines, we can further identify a rather broad band between  $900 \text{ cm}^{-1}$  and  $975 \text{ cm}^{-1}$  (see also inset of Fig. 8). The intensity of this band increases as the Ce content in the films increases thus suggesting that this feature is related to the presence of Ce. In the literature,<sup>24,25</sup> several closely spaced peaks have been identified in the range  $826\text{-}975 \text{ cm}^{-1}$ , which may be due to the formation of

the  $\text{Ce}_2\text{Si}_2\text{O}_7$  or  $\text{Ce}_{4.667}(\text{SiO}_4)_3\text{O}$  compounds. Our FTIR investigations thus confirm the formation of a cerium silicate for high annealing temperatures.

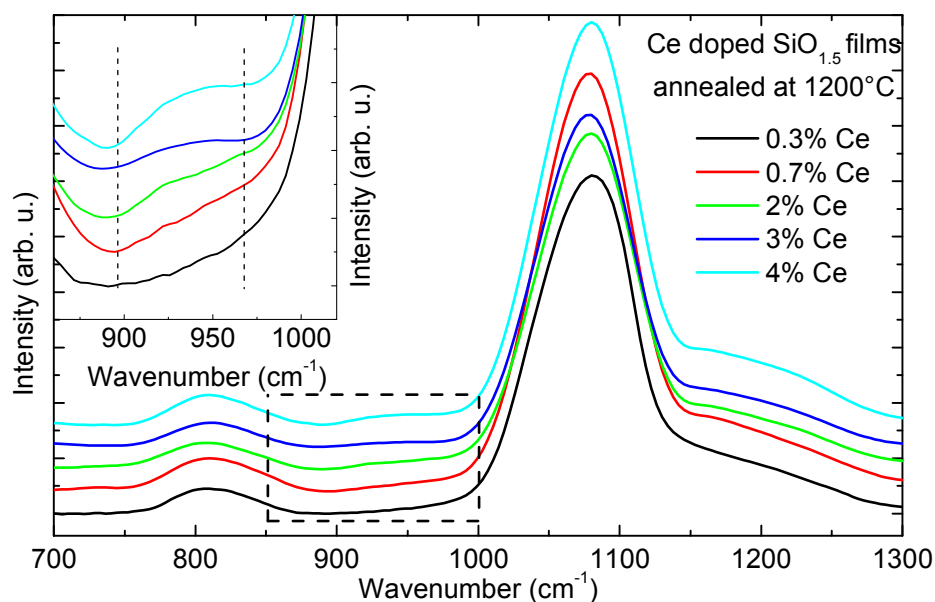


**Fig.8** FTIR spectra of Ce-doped  $\text{SiO}_{1.5}$  thin films annealed at  $1200^\circ\text{C}$ . The Ce content is varied between 0.3 % and 4 %. All spectra are vertically offset for clarity. The dashed area is enlarged in the inset. The vertical dashed lines in the inset indicate the wavenumber range in which features corresponding to the formation of a cerium silicate are expected.

Finally, we will discuss the general evolution observed during annealing of Ce-doped  $\text{SiO}_{1.5}$  thin films. Atom probe tomography measurements performed on the as-grown films show that Ce atoms are almost randomly distributed (not shown here). When the samples are annealed at  $900^\circ\text{C}$ , amorphous Ce-rich clusters have been identified by both STEM (Fig. 3) and APT measurements (Fig. 4). This indicates that Ce diffusion is thermally activated in our films. Moreover, as the annealing temperature increases up to  $900^\circ\text{C}$ , a demixtion occurs in the  $\text{SiO}_{1.5}$  films leading to Si atoms in excess in a matrix with a composition reaching  $\text{SiO}_2$ . Both Ce and Si atoms will then diffuse and eventually accumulate at the pores/vacancies of the films thus leading to Ce- and Si-rich clusters as shown in Fig. 4(c). At least up to the

annealing temperature of 900°C, the evolution appears to be essentially governed by kinetics, i.e. by diffusion and clustering of both Si and Ce. When the films are further annealed at higher temperatures, thermodynamics takes over and the Si-O-Ce system will move towards stable compounds. The formation of cerium silicates is, however, precluded at 900°C since the thermal budget is still too low.<sup>21</sup> According to the Ce-Si phase diagram,<sup>26</sup> the formation of cerium silicides appears also to be unlikely for the Ce contents and annealing temperatures considered in our study. Moreover, we can also rule out the formation of CeO<sub>2</sub> since we do not observe the well-known Raman peak at 462 cm<sup>-1</sup> in Fig. 5. This conclusion is further supported by the X-ray photoelectron spectroscopy data which do not show a significant increase of the Ce<sup>4+</sup> related peak intensities as the annealing temperature increases. For annealing temperatures above 980°C, the formation of cerium silicates such as Ce<sub>2</sub>Si<sub>2</sub>O<sub>7</sub> or Ce<sub>4.667</sub>(SiO<sub>4</sub>)<sub>3</sub>O starts. At this temperature, compositional analysis based on APT measurements have shown that the Si content in the clusters is about 24 %, which is much larger than the amount of Si required to form the cerium silicates (i.e. 18.2 % for Ce<sub>2</sub>Si<sub>2</sub>O<sub>7</sub> and 14.5 % for Ce<sub>4.667</sub>(SiO<sub>4</sub>)<sub>3</sub>O). Consequently, the Si atoms in excess will be ejected and will agglomerate to form pure Si nanocrystals at the immediate vicinity of the cerium silicate clusters. We thus expect that thermodynamics is the main driving force leading to the formation of stable phases which in our case are Si, SiO<sub>2</sub> and Ce<sub>2</sub>Si<sub>2</sub>O<sub>7</sub> or Ce<sub>4.667</sub>(SiO<sub>4</sub>)<sub>3</sub>O.

## Conclusions

To summarize, we have investigated both the structural and optical properties of Ce-doped SiO<sub>1.5</sub> thin films. The complex evolution of the Ce-related luminescence with the annealing temperature is well explained thanks to a complementarity of different nanoscale structural characterizations and vibrational spectroscopies. In particular, the strong PL decrease at 900°C is related to the presence of Ce-rich clusters. At higher annealing

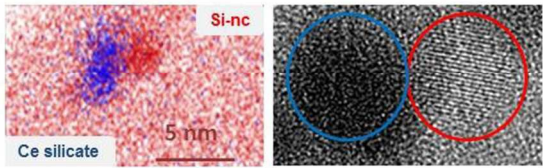
temperatures, we were able to identify and characterize a phase separation occurring at a length scale below 10 nm between pure Si nanocrystals and Ce-rich clusters having a stoichiometry close to  $\text{Ce}_2\text{Si}_2\text{O}_7$  or  $\text{Ce}_{4.667}(\text{SiO}_4)_3\text{O}$ . This is the first direct observation of a nanoscale phase separation in a solid state matrix. The cerium silicates are known to be luminescent thereby explaining the increased Ce-related luminescence at 1100°C. At the present stage of our investigations, the microscopic driving force at the origin of the observed phase separation is not yet clearly identified. Further theoretical work using kinetic Monte Carlo simulations and/or even molecular dynamics or nano-thermodynamic simulations would be needed to clarify this important issue. This work brings a comprehensive view of the optical properties of Ce-doped Si-based layers in relation with its structure and then represents an important step towards the realization of blue light emitting devices fully compatible with the well-known Si technology.

## Notes and references

- 1 S. Takeoka, M. Fujii and S. Hayashi, *Phys. Stat. Sol. B*, 2001, **224**, 229-232.
- 2 G. Scardera, T. Puzzer, I. Perez-Wurfl and G. Conibeer, *J. Cryst. Growth*, 2008, **310**, 3680-3684.
- 3 M. Zacharias, J. Heitmann, R. Scholz, U. Kahler, M. Schmidt and J. Blasing, *Appl. Phys. Lett.*, 2002, **80**, 661-663.
- 4 O. Jambois, H. Rinnert, X. Devaux and M. Vergnat, *J. Appl. Phys.*, 2005, **98**, 046105(1)-046105(3).
- 5 M. Fujii, M. Yoshida, Y. Kanzawa, S. Hayashi and K. Yamamoto, *Appl. Phys. Lett.*, 1997, **71**, 1198-1200.
- 6 E. Steveler, H. Rinnert and M. Vergnat, *J. Appl. Phys.*, 2011, **110**, 113518(1)-113518(4).

- 7 C. H. Liang, J. Cardin, C. Labbe and F. Gourbilleau, *J. Appl. Phys.*, 2013, **114**, 033103(1)-033103(8).
- 8 A. H. Morshed, M. E. Moussa, S. M. Bedair, R. Leonard, S. X. Liu and N. El-Masry, *Appl. Phys. Lett.*, 1997, **70**, 1647-1649.
- 9 W. C. Choi, H. N. Lee, E. K. Kim, Y. Kim, C. Y. Park, H. S. Kim and J. Y. Lee, *Appl. Phys. Lett.*, 1999, **75**, 2389-2391.
- 10 L. Kepinski, D. Hreniak and W. Strek, *J. Alloys Compd.*, 2002, **341**, 203-207.
- 11 J. Li, O. Zalloum, T. Roschuk, C. Heng, J. Wojcik and P. Mascher, *Appl. Phys. Lett.*, 2009, **94**, 011112(1)-011112(3).
- 12 J. Weimmskirch-Aubatin, M. Stoffel, X. Devaux, A. Bouché, M. Vergnat and H. Rinnert, *Phys. Stat. Sol. C*, 2014, **11**, 1630-1633.
- 13 J. Weimmskirch-Aubatin, M. Stoffel, A. Bouché, P. Boulet, M. Vergnat and H. Rinnert, *J. Alloys Compd.*, 2015, **622**, 358-361.
- 14 K. Thompson, D. Lawrence, D. Larson, J. Olson, T. Kelly and B. Gorman, *Ultramicroscopy*, 2007, **107**, 131-139.
- 15 E. Talbot, R. Lardé, F. Gourbilleau, C. Dufour and P. Pareige, *Europhys. Lett.*, 2009, **87**, 26004(1)-26004(5).
- 16 A. Pfau and K. D. Schierbaum, *Surf. Sci.*, 1994, **321**, 71-80.
- 17 E. J. Preisler, O. J. Marsh, R. A. Beach and T. C. McGill, *J. Vac. Sci. Technol. B*, 2001, **19**, 1611-1618.
- 18 M. Seah, *Surf. Sci.*, 1999, **420**, 285-294.
- 19 M. Seah, I. Gilmore and S. Spencer, *Surf. Sci.*, 2000, **461**, 1-15.
- 20 H. Rinnert, M. Vergnat and A. Burneau, *J. Appl. Phys.*, 2001, **89**, 237-243.
- 21 A. Cuneyt Tas and M. Akinc, *J. Am. Ceram. Soc.*, 1994, **77**, 2953-2960.
- 22 S. Y. Lin, *J. Appl. Phys.*, 1997, **82**, 5976-5982.

- 23 H. Z. Song, X. M. Bao, N. S. Li and X. L. Wu, *Appl. Phys. Lett.*, 1998, **72**, 356-358.
- 24 L. Kepinski, M. Wolcyrz and M. Marchewka, *J. Solid State Chem.*, 2002, **168**, 110-118.
- 25 I. F. Andreev, A. N. Sokolov, A. M. Shebyakov, Y. P. Tarlakov and N. A. Toropov , *J. Appl. Spectros.*, 1971, **14**, 263-265.
- 26 M. V. Bulanova, P. N. Zheltov, K. A. Meleshevich, P. A. Saltykov and G. Effenberg, *J. Alloys Compd.*, 2002, **345**, 110-115.



254x190mm (96 x 96 DPI)